

Comparison of the Electrochemical Behavior of Ti and Nanostructured Ti-Coated AISI 304 Stainless Steel in Strongly Acidic Solutions



FARID REZA ATTARZADEH, HASSAN ELMKHAH,
and ARASH FATTAH-ALHOSSEINI

In this study, the electrochemical behaviors of pure titanium (Ti) and nanostructured (NS) Ti-coated AISI 304 stainless steel (SS) in strongly acidic solutions of H_2SO_4 were investigated and compared. A type of physical vapor deposition method, cathodic arc evaporation, was applied to deposit NS Ti on 304 SS. Scanning electron microscope and X-ray diffraction were used to characterize surface coating morphology. Potentiodynamic polarization, electrochemical impedance spectroscopy, and Mott–Schottky (M–S) analysis were used to evaluate the passive behavior of the samples. Electrochemical measurements revealed that the passive behavior of NS Ti coating was better than that of pure Ti in 0.1 and 0.01 M H_2SO_4 solutions. M–S analysis indicated that the passive films behaved as n-type semiconductors in H_2SO_4 solutions and the deposition method did not affect the semiconducting type of passive films formed on the coated samples. In addition, this analysis showed that the NS Ti coating had lower donor densities. Finally, all electrochemical tests showed that the passive behavior of the Ti-coated samples was superior, mainly due to the formation of thicker, yet less defective passive films.

DOI: 10.1007/s11663-016-0837-0

© The Minerals, Metals & Materials Society and ASM International 2016

I. INTRODUCTION

VARIOUS physical vapor deposition (PVD) techniques such as unbalanced magnetron sputtering,^[1] high-power impulse magnetron sputtering,^[2] pulsed laser deposition,^[3] arc ion plating,^[4] and the like have been applied to deposit pure titanium (Ti) and Ti-based ceramic coatings, *e.g.*, TiN, TiAlN, and TiC. In particular, cathodic arc evaporation (CAE) is a commercialized method in which a high-rate and dense deposition is attainable without heating the substrate.^[5,6] In response to the requirements of industries for highly corrosion-resistant materials, PVD methods have been developed for the deposition of protective coatings.^[7,8] Such coatings must be either cathodically protecting or defect-free and inert to be applied as corrosion protective coatings. Formation of a nearly defect-free and inert coating is considered to be the case discussed herein. Moreover, the structure of coating may have a profound impact on its protective properties. A study of literature shows that

nano-grained or amorphous metals may offer more uniform and predictable sacrificial corrosion protection, essentially due to their small and uniformly distributed features.^[9] According to Thornton's structure zone model,^[10,11] PVD coating in the low temperature and low inert gas pressure deposits a fine grain size structure. In the PVD technique, it is possible to achieve nanostructured (NS) coatings.^[12,13]

However, the main disadvantages of the coatings prepared by the CAE are the presence of porosity, pin holes, droplets, and other macro/micro surface defects which can adversely affect the passivation and corrosion resistance. In fact, some parts of the substrate may not be readily covered by the protective layer or surface defects may present serious pitting attacks.^[14,15] On the bright side, applying double- or multilayer coatings not only improves the tribological properties of the coatings but also eliminates these defects to a large extent, thereby enhancing the corrosion resistance of the final product. Liu *et al.* have reported that a thin, yet well-bonded interlayer of Ti or TiN reduces the corrosion attacks effectively and modifies the pit propagation mechanism.^[16]

The purpose of the current study was twofold: first, a controlled two-step coating of Ti on the surface of 304 stainless steel (SS); second, comparing the passive behavior of pure Ti and NS Ti coating in strongly acidic solutions of H_2SO_4 . It should be noted that the relatively thick coating that obtained herein renders the samples totally covered. Accordingly, the electrochemical behavior of Ti-coated samples was compared to the pure Ti rather than the underlying 304 SS substrate.

FARID REZA ATTARZADEH, Junior Engineer, is with the Research Institute of Petroleum Industry, Corrosion Division, Tehran, 14857-33111, Iran. Contact e-mail: a.fattah@basu.ac.ir, HASSAN ELMKHAH and ARASH FATTAH-ALHOSSEINI, Assistant Professors, are with Department of Materials Engineering, Bu-Ali Sina University, Hamedan 65178-38695, Iran.

Manuscript submitted July 27, 2016

Article published online October 14, 2016.

II. MATERIALS AND METHODS

A. Sample Processing

The AISI 304 SS specimens were first ultrasonically cleaned in acetone and ethanol for 10 minutes. Then glow discharge was applied in a vacuum chamber for super-cleaning. For this purpose, a pulsed bias voltage of -800 V at 80 pct duty cycle in the Ar atmosphere was applied for 3 minutes.

Then, the Ti interlayer and main coating were deposited *via* CAE technique at the constant working condition including the frequency of 1000 Hz, the distance between substrate and target of 140 mm, and a bias voltage of -100 V. For the sake of brevity, other deposition parameters are summarized in Table I. A high-purity Ti target (99.95 wt pct) was used as the cathode for both consecutive steps of depositions. It is worth mentioning that a similar procedure was used

Table I. Conditions of PVD-Ti Deposition and Its Interlayer

Parameters	Interlayer	Ti coating
Target (pct)	Ti (99.95)	Ti (99.95)
Working pressure	0.0106657896 Pa (8×10^{-5} Torr)	0.39996711 Pa (3×10^{-3} Torr)
Target current (A)	120	100
Deposition time (min)	2	30
Deposition temperature	398 K (100 °C)	448 K (150 °C)
Duty cycle (pct)	50	80

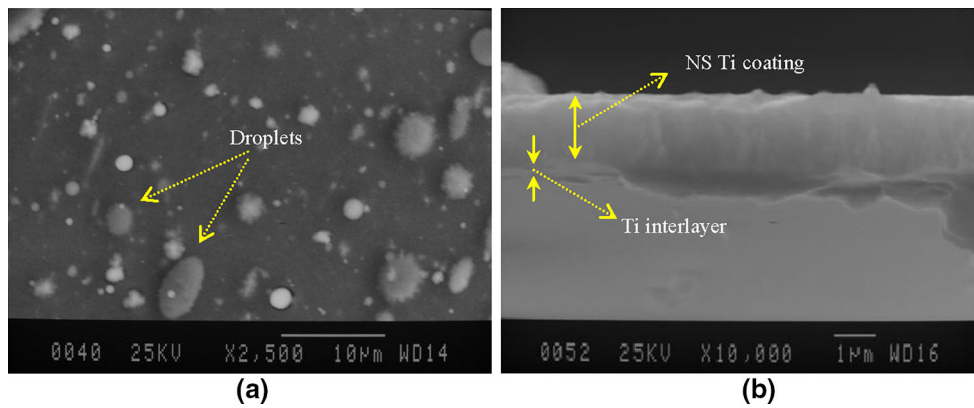


Fig. 1—SEM images of the nanostructured Ti-coated 304 SS: (a) morphology of the surface and (b) cross section of the coating.

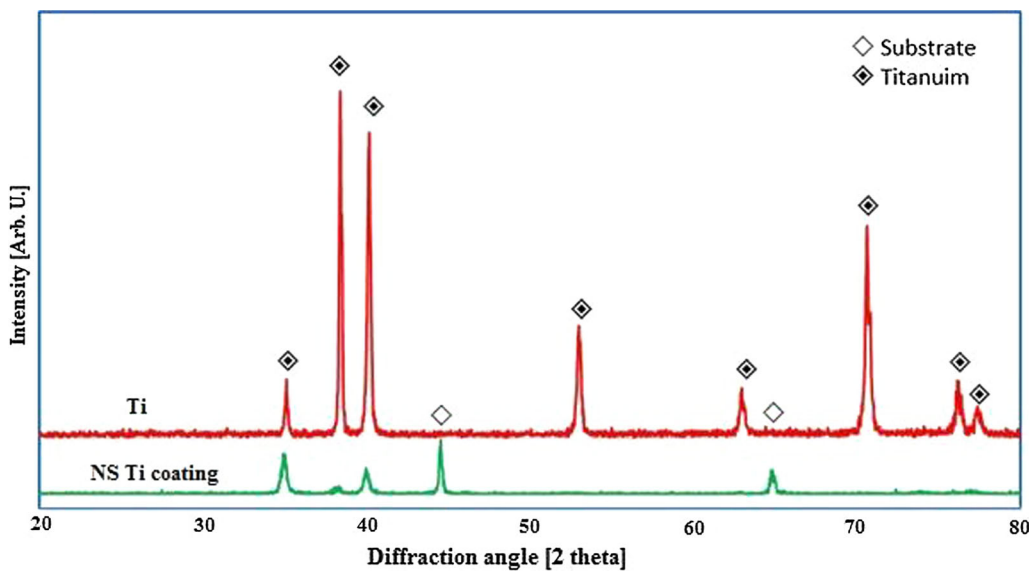
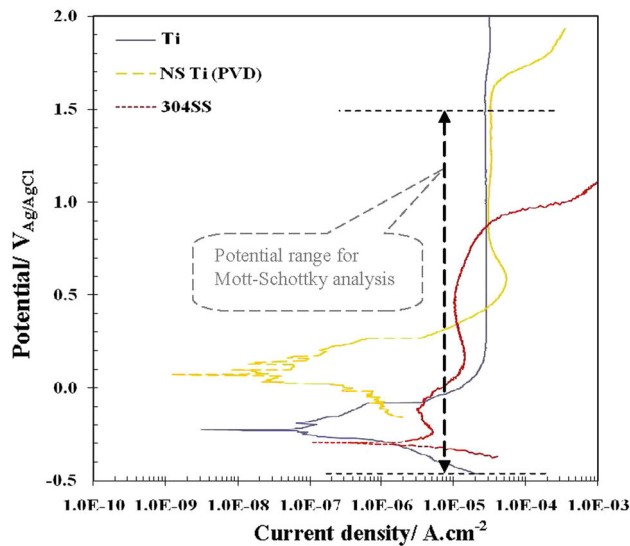


Fig. 2—XRD patterns of the Ti and nanostructured (NS) Ti-coated 304 SS.

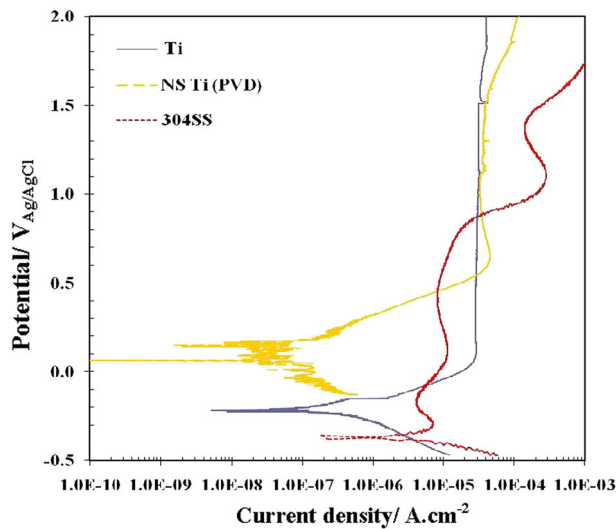
previously to deposit an ultrathin Ti film on silicon wafers but for a much shorter time.^[17]

B. Microstructural Characterization

Scanning electron microscope (SEM) micrographs of NS Ti-coated sample were obtained by a JEOL JSM-840A SEM. Top view was used to investigate the surface morphology. Cross-section view was used to estimate the coating thickness and check its integrity. Phase identification of the Ti and NS Ti coatings was performed using X-ray diffraction (XRD) analysis [Italstructures APD2000 diffractometer, operating at 40 kV and 40 mA with Cu K α radiation ($\lambda = 0.1506$ nm)]. The XRD patterns were recorded in the range of $2\theta = 20$ to 80 deg using a step size of 0.02 deg and a counting time of 1 second per step.



(a)



(b)

Fig. 3—Potentiodynamic polarization curves of 304 SS, Ti, and nanostructured Ti-coated 304 SS in H₂SO₄ solutions: (a) 0.1 M H₂SO₄ (pH 1) and (b) 0.01 M H₂SO₄ (pH 2).

C. Electrochemical Testing

Before any electrochemical tests, 304 SS and Ti samples were ground to 2000 grit and cleaned with deionized water. Then, the tests were carried out at $298 \text{ K} \pm 1 \text{ K}$ ($25 \text{ }^\circ\text{C} \pm 1 \text{ }^\circ\text{C}$) in a three-electrode flat cell configuration: working electrode (304 SS/Ti/NS Ti-coated samples) + counter electrode (a Pt wire) + reference electrode [Ag/AgCl saturated in KCl]. A μ Autolab Type III/FRA2 system was used for all electrochemical tests. Two different aerated acid solutions of 0.01 (pH 2) and 0.1 M H₂SO₄ (pH 1) were prepared from analytical grade 97 pct H₂SO₄ and distilled water.

The working electrode was immersed at open circuit potential (OCP) prior to any electrochemical measurements in 0.1 and 0.01 M H₂SO₄ (pH 1 and 2, respectively) solutions for 1800 seconds in order to ensure that the steady state was established. Potentiodynamic polarization curves were obtained (scan rate = 1 mV s^{-1}) starting from -0.25 V (*vs* E_{corr}) to $4.0 \text{ V}_{\text{Ag/AgCl}}$. Electrochemical impedance spectroscopy (EIS) measurements were performed at OCP and AC potential with the amplitude of 10 mV and the frequency range of 100 kHz to 10 mHz. To validate the impedance spectra, the linearity condition was taken into account by measuring the spectra at AC signal amplitudes between 5 and 15 mV (rms). Additionally, Kramers–Kronig (K–K) transforms were applied to validate and guarantee the experimental measurements and stability conditions. For the EIS data modeling, the curve-fitting method, and K–K test, NOVA 1.7.8 impedance software was used. Finally, Mott–Schottky (M–S) analysis was carried out on the passive films using a 10 mV AC signal in the cathodic direction (frequency = 1 kHz and step potential = 25 mV).

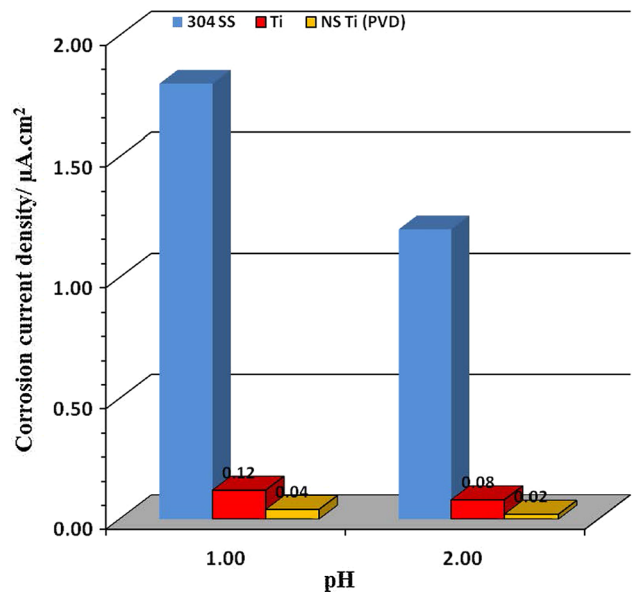


Fig. 4—Corrosion current densities of 304 SS, Ti, and nanostructured Ti-coated 304 SS in H₂SO₄ solutions.

III. RESULTS AND DISCUSSION

A. Microstructural Evolutions

Figure 1 shows the SEM micrographs of the NS Ti-coated sample, which includes both top and cross-section views. Although the existence of macro-droplets on the surface is a common feature of coatings deposited by the CAE method,^[18] the amount of these contaminations was controlled by adjusting the working pressure range and the distance between cathode and the sample. In addition, the coating thickness was estimated to be around 2 μm . Figure 2 shows the XRD patterns of the Ti and the NS Ti-coated samples. The full width at half maximum (FWHM) for each sample was measured through the XRD patterns and, subsequently, the crystallite size of the coating was obtained by the Scherrer formula (Eq. [1]):^[19,20]

$$D = \frac{0.94 \times \lambda}{(\beta^2 - \beta_i^2)^{0.5} \cdot \cos \theta}, \quad [1]$$

where D is the crystallite size, β is the FWHM of the diffraction peak (rad), β_i is the broadened peak due to

micro-strain effect, λ is the wavelength (1.540 \AA) of the incident Cu $K\alpha$ X-ray, and θ is the diffraction angle. Since the crystallite size is inversely proportional to the FWHM value of the highest peak, it can be said that the higher the amount of FWHM, the smaller the crystallite size. Considering the above equation, the estimated crystallite size of the coating was found to be ~ 20 nm. Not to mention, the grain size of the Ti sample is in the micrometer range. As it is indicated in Figure 2, two specific peaks can be attributed to the 304 SS substrate. Other peaks belong to the NS Ti coating, which are clearly broadened compared to the ones observed for Ti. Besides, (100) orientation emerges as the preferred orientation of NS Ti coating. It is also worth mentioning that both the preferred orientation and size effect (peak broadening) are responsible for the disappearance of some Ti peaks.

B. Potentiodynamic Polarization Measurements

Polarization curves of the 304 SS, pure Ti, and NS Ti-coated samples in H_2SO_4 solutions are shown in Figure 3. As can be seen, the corrosion potentials shifted

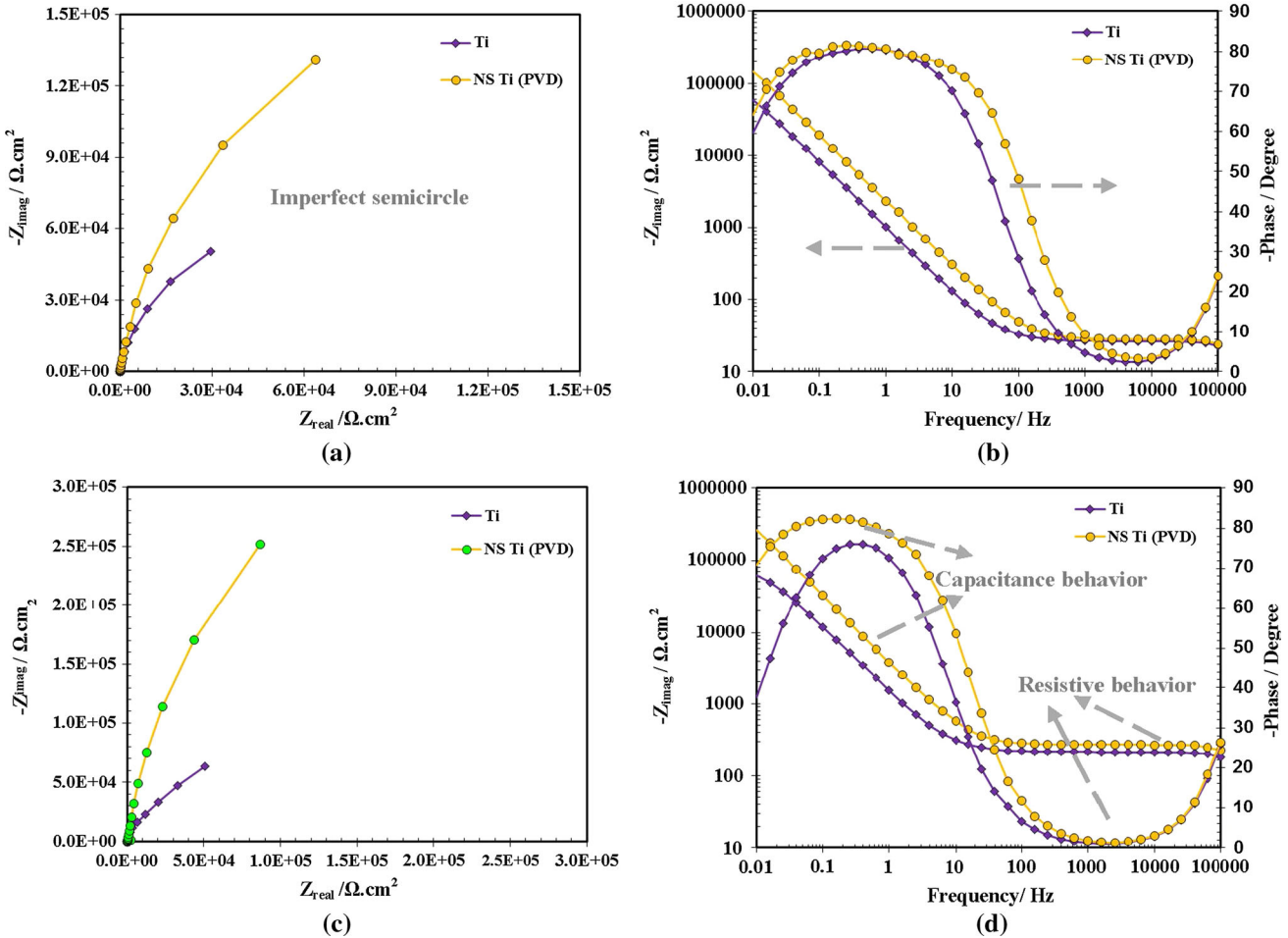


Fig. 5—Nyquist and Bode plots for Ti and nanostructured Ti-coated 304 SS in sulfuric acid solutions: (a, b) 0.1 M H_2SO_4 (pH 1) and (c, d) 0.01 M H_2SO_4 (pH 2).

to higher and slightly positive values for NS Ti coating. This shift is more pronounced when the pH is 1 or the H_2SO_4 concentration is 0.1 M (Figure 3(a)). More importantly, neither any jump nor any abrupt increase in the anodic current density can be witnessed for NS Ti coating in both acid solutions. Furthermore, Tafel extrapolation was considered for the estimation of corrosion current densities.^[21] For clarity, corrosion current densities derived from the above curves are shown in Figure 4 in the form of a histogram. It is observed that NS Ti-coated samples have lower corrosion current densities compared to Ti and 304 SS samples encountering both acid solutions. As it is expected, the corrosion current densities are lower for a higher pH value, *i.e.*, pH value of 2. Similar potentiodynamic polarization curves were observed for Ti in 0.1 M HCl solution.^[22] The NS Ti coating seems to protect its underlying substrate well and even its passive behavior surpasses Ti, albeit this inference needs further investigation.

C. EIS Measurements

The Nyquist, Bode phase, and Bode magnitude plots of Ti and NS Ti-coated samples in H_2SO_4 solutions are

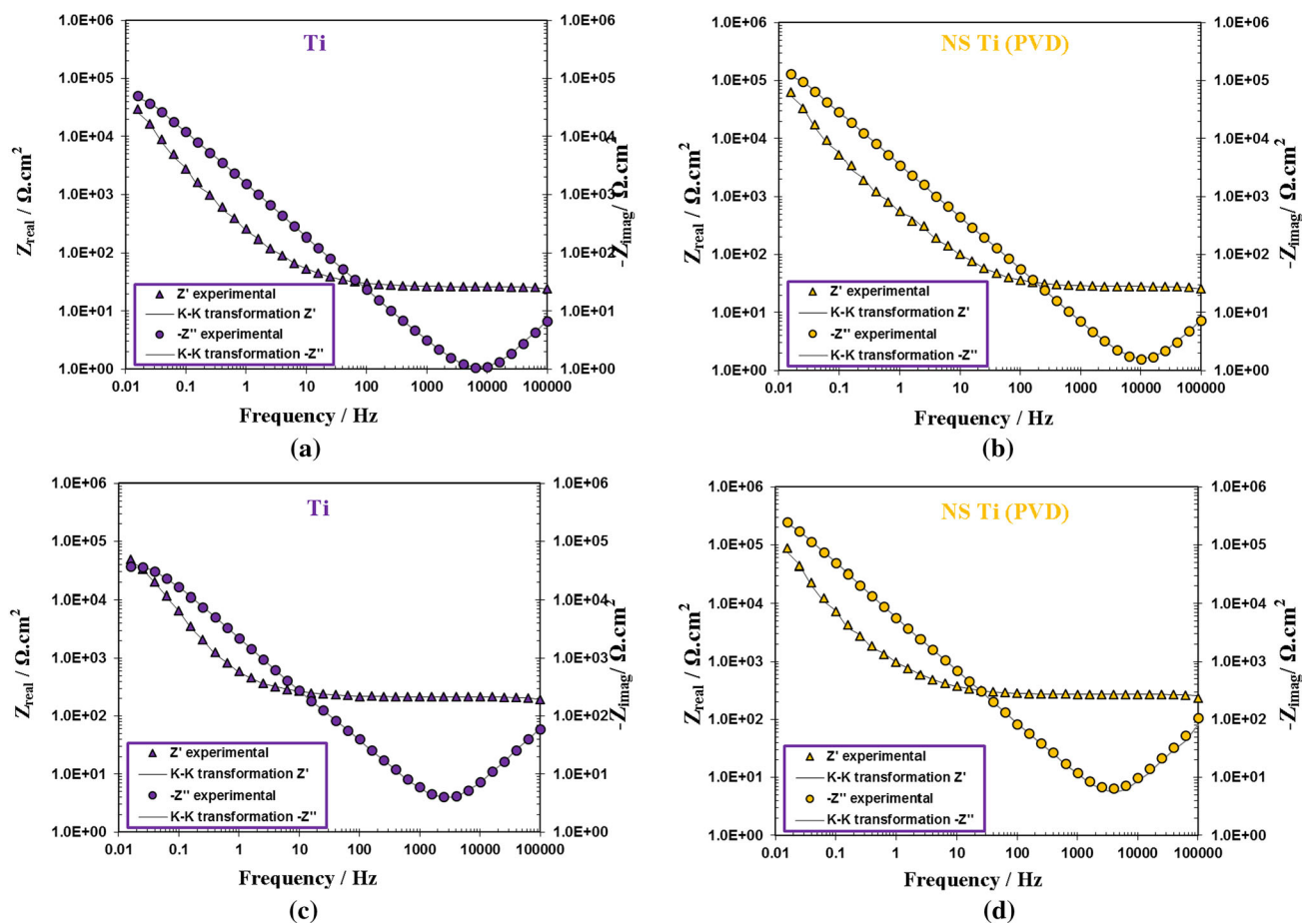


Fig. 6—Kramers–Kronig transformation of the EIS data obtained for (a) Ti in 0.1 M H_2SO_4 (pH 1), (b) nanostructured Ti-coated 304 SS in 0.1 M H_2SO_4 (pH 1), (c) Ti in 0.01 M H_2SO_4 (pH 2), and (d) nanostructured Ti-coated 304 SS in 0.01 M H_2SO_4 (pH 2).

all illustrated in Figure 5. Figures 5(a) and (b) show the EIS plots of both samples in 0.1 M H_2SO_4 solution (pH 1), while Figures 5(c) and (d) show the EIS plots of both samples in 0.01 M H_2SO_4 solution (pH 2). At first glance, neither any other capacitive loop nor any linear range in the high-frequency domain would be seen in the Nyquist plots (Figures 5(a) and (c)). Thus, the dissolution of substrate or a Warburg behavior is not expected as reported in the earlier studies conducted by Creus *et al.*^[15] Nyquist plots (Figures 5(a) and (c)) demonstrate imperfect semicircles. Since the diameters of these semicircles are directly proportional to the overall resistance, the NS Ti-coated sample has a higher

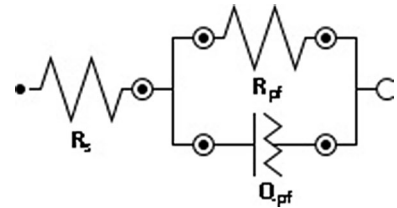


Fig. 7—Equivalent electrical circuits used to model the experimental EIS data.

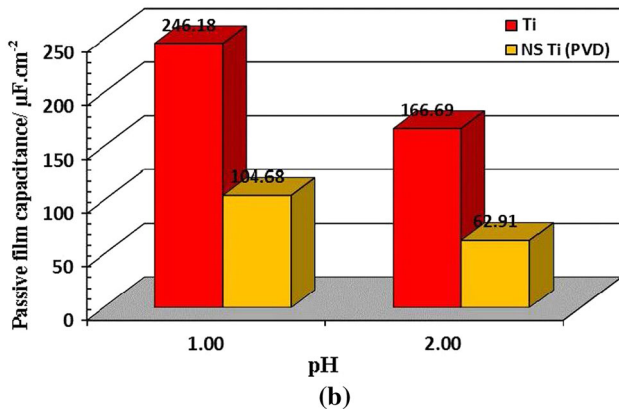
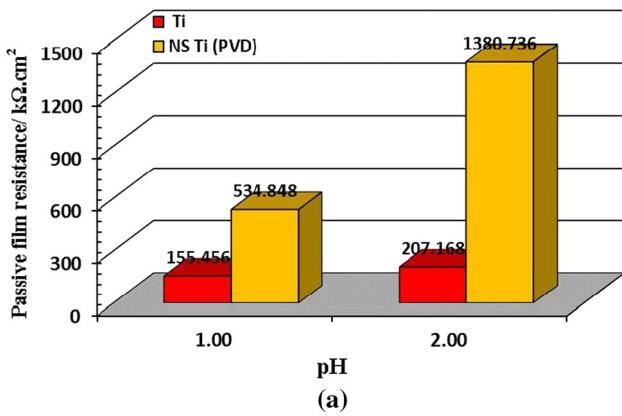


Fig. 8—(a) Passive film resistance and (b) passive film capacitance of Ti and nanostructured Ti-coated 304 SS in H₂SO₄ solutions.

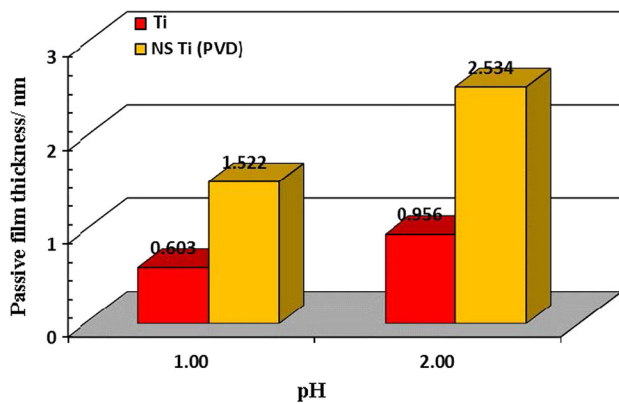


Fig. 9—Calculated passive film thickness of Ti and nanostructured Ti-coated 304 SS in H₂SO₄ solutions.

resistance in both acid solutions. Moreover, Bode plots (Figures 5(b) and (d)) exhibit a resistive behavior in the high-frequency range, whereas a marked capacitive response can be witnessed in the middle-to-low frequency range. It is also worth noting that the electrochemical differences between the samples are more observable when the pH is 2 (0.01 M H₂SO₄ solution). Considering the Bode phase plots presented in

Figures 5(b) and (d), a constant phase behavior can be inferred in the intermediate frequency range. The phase angle values remained very close to -80 deg and revealed that a highly stable passive film was formed on the surface of NS Ti coating.

It should be noted that the validity of impedance data necessitates electrochemical systems satisfying the constraints of linear system theory, namely causality, linearity, and stability. Accordingly, K–K transforms were applied by transforming the real axis to the imaginary axis and vice versa. A detailed description of K–K transforms as well as accompanied formulations can be found in References 24 and 25. The EIS experimental data of both Ti and NS Ti-coated samples in H₂SO₄ solutions were compared with those obtained from K–K transforms (Figure 6). The obtained results confirmed the agreement between the experimental data and K–K transforms, which accorded well with the linear system theory.

On the basis of Bode plots depicted in Figures 5(b) and (d), a single time constant can be considered for the EIS spectra of both Ti and NS Ti-coated samples. Thus, an equivalent electrical circuit (EEC) shown in Figure 7 can be used for the modeling and simulation of impedance spectra. It is not uncommon to use Randles circuit for Ti PVD coatings as it was suggested before to describe the electrochemical behavior of a PVD film of Ti on AISI 316L SS substrate in NaCl 9 g L⁻¹ solution.^[26] The elements of the above EEC are defined as follows: R_s is the solution resistance, R_{pf} stands for the resistance of the passive film, and Q_{pf} is the constant phase element (CPE) corresponding to the capacitance of the passive film. The impedance and the capacitance of the CPE can be calculated using Eqs. [2] and [3], respectively.^[22,27]

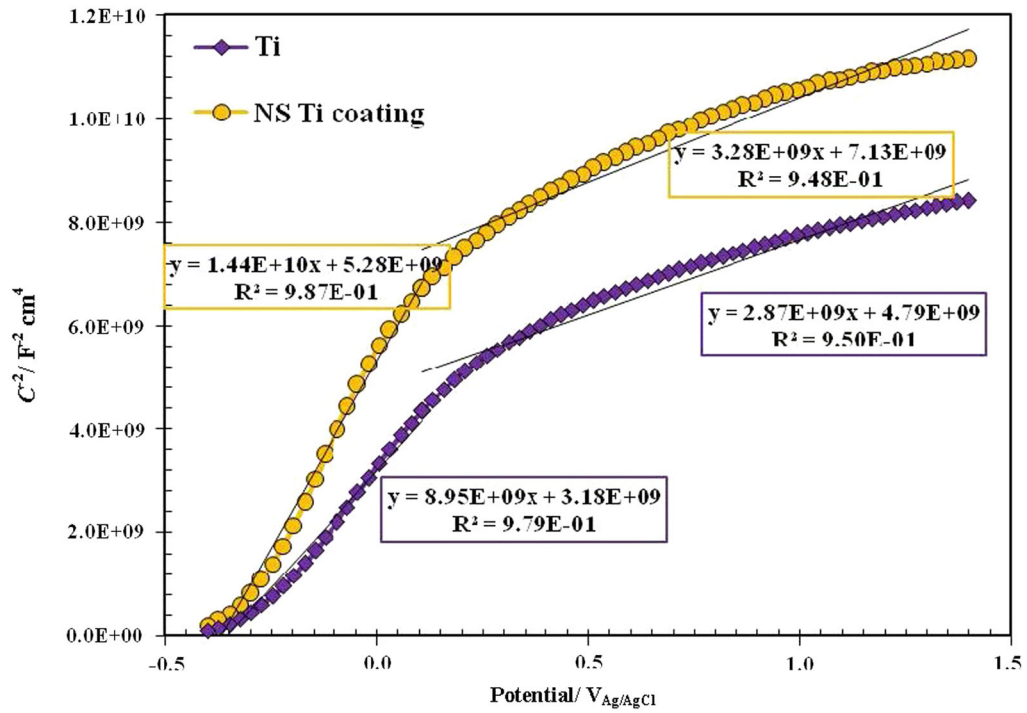
$$Z_{CPE} = [Q(j\omega)^n]^{-1}, \quad [2]$$

where ω is the angular frequency (rad s⁻¹), Q is the CPE constant, j is the imaginary unit, and n is the CPE exponent that ranges from 0 to 1 and may provide information regarding surface roughness and surface inhomogeneity. On the other hand, the second aforementioned equation is expressed as follows:

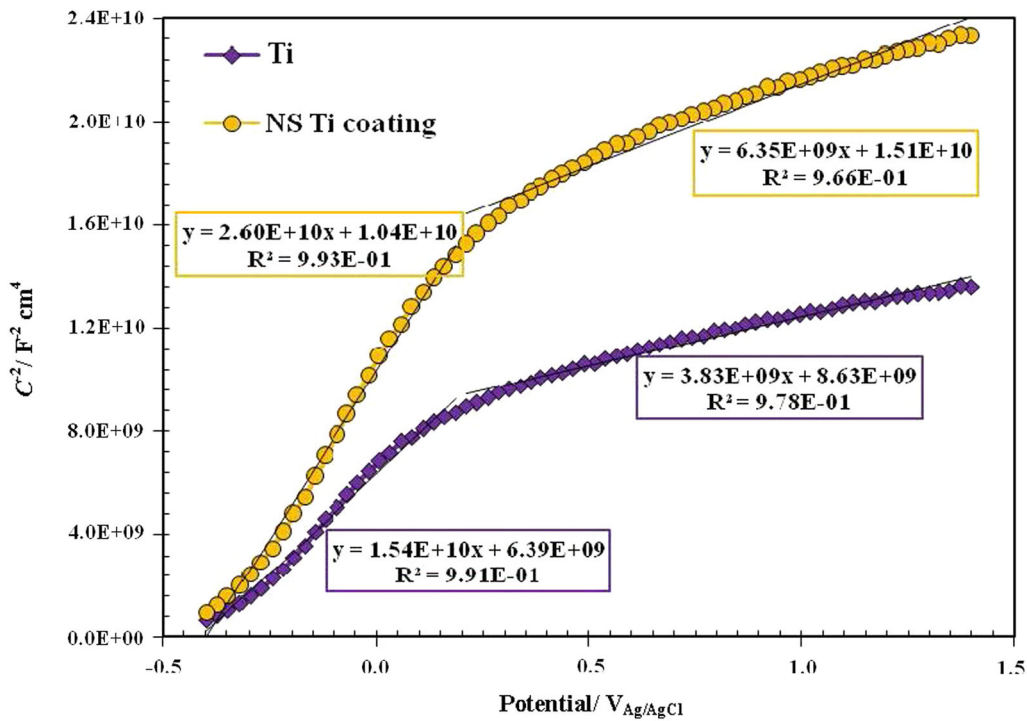
$$C = Y_0(\omega_{\max})^{n-1}, \quad [3]$$

where Y_0 is the admittance and ω_{\max} is the angular frequency at which the maximum in the imaginary component of the impedance occurs.

The variation of resistance and capacitance of the passive films formed on Ti and NS Ti-coated samples in H₂SO₄ solutions are illustrated in Figure 8. It can be seen that the passive film resistances of both samples are lower when the pH is 1 (Figure 8(a)). Additionally, the NS Ti-coated sample has a higher passive film resistance compared to that of Ti sample at both pH values. On the other hand, Figure 8(b) shows that the passive film capacitance of the Ti sample is higher than that of the NS Ti-coated sample. This figure also shows that the passive film capacitance decreases for both samples when the pH value is 2.



(a)



(b)

Fig. 10—Mott-Schottky plots of Ti and nanostructured Ti-coated 304 SS in sulfuric acid solutions: (a) 0.1 M H₂SO₄ (pH 1) and (b) 0.01 M H₂SO₄ (pH 2).

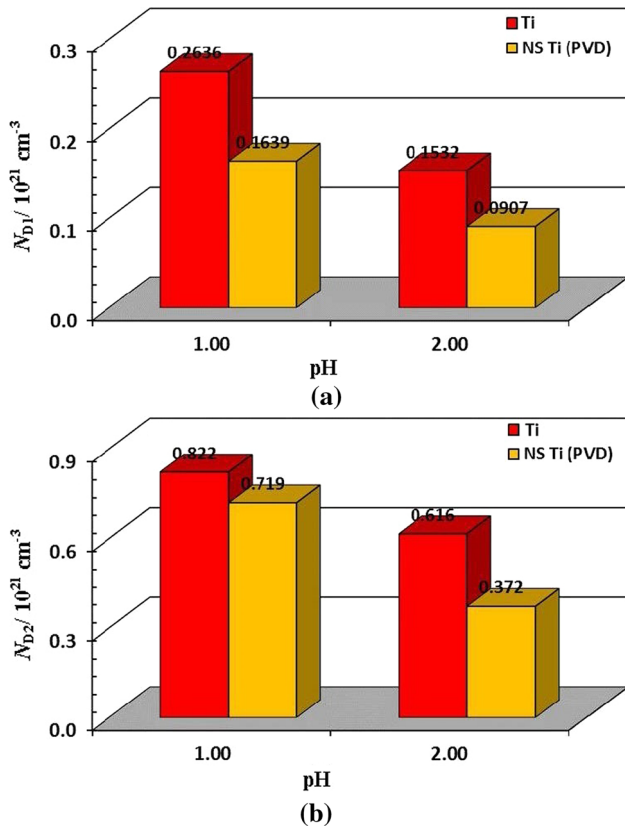


Fig. 11—Calculated donor densities of the passive films formed on Ti and nanostructured Ti-coated 304 SS in H_2SO_4 solutions: (a) N_{A1} and (b) N_{A2} .

Furthermore, the passive film thickness can be calculated using Eq. [4]:^[27,28]

$$L = \frac{\varepsilon\varepsilon_0 A}{C}, \quad [4]$$

where L is the passive film thickness, C is the passive film capacitance, ε is the passive film dielectric constant (usually taken as 60^[28]), ε_0 is the vacuum permittivity ($8.854 \times 10^{-14} \text{ F cm}^{-1}$), and A denotes the effective area (normally two–three times that of the apparent geometric surface area^[29]). Equation [4] implies that there is an inverse relationship between the passive film capacitance and passive film thickness. Figure 9 shows the variation of the passive film thickness (L) of Ti and NS Ti-coated samples in H_2SO_4 solutions. The calculated passive film thickness is in the range of 1 to 2 nm, which is comparable to those of reported values in the literature for Ti in acidic solutions.^[28,30] It can be seen that NS Ti-coated sample has a thicker passive film compared to Ti. Therefore, nanostructuring of Ti coating promotes the formation of a thicker and more protective passive film in H_2SO_4 media.

D. Mott–Schottky Analysis

The M–S plots of Ti and NS Ti-coated samples are shown in Figure 10. It is observable that as the potential increases, the inverse square of space charge capacitance (C_{sc}^{-2}) increases monotonically for both samples. In all M–S plots, C_{sc}^{-2} and E possess a near-linear relationship in two regions. The observed positive slopes in these regions can be unequivocally ascribed to an n-type semiconducting behavior. Similar M–S plots have been reported for Ti in acidic solutions.^[22,29] According to Eq. [5], the donor densities were estimated from these positive slopes:^[30]

$$\frac{1}{C_{sc}^2} = \frac{2}{\varepsilon\varepsilon_0 e N_D} \left(E - E_{fb} - \frac{k_B T}{e} \right), \quad [5]$$

where e stands for the electron charge, N_D is the donor density for an n-type semiconductor (cm^{-3}), and k , T , and E_{fb} are the Boltzmann constant, absolute temperature, and flat band potential, respectively.

Figure 11 shows the estimated donor densities (N_{A1} and N_{A2}) of Ti and NS Ti-coated samples in H_2SO_4 solutions. N_{A1} is calculated for the low-potential region near flat band potential, while N_{A2} is calculated for high-potential region of M–S plots. According to this figure, NS Ti-coated sample has lower donor densities in both acid solutions. In addition, both samples have lower donor densities at pH 2 or the equivalent H_2SO_4 concentration of 0.01 M. The donor densities are in the order of 10^{21} cm^{-3} which are comparable to the values reported elsewhere.^[28,31] Here it should be emphasized that the presence of multiple slopes in M–S plots has been interpreted differently in the literature. The suppositions offered are inhomogeneity of donor distribution, the presence of surface states, a change in the donor type and/or donor density with potential, or the presence of second donor level in the band gap, which is related to the partial ionization of deep donors.^[27]

However, according to the point defect model (PDM) for Ti in acidic solutions (Figure 12), the oxygen vacancies and/or the cation interstitials act as electron donors and, hence, lead to an n-type semiconducting behavior of the passive film.^[32,33] A higher density of the oxygen vacancies and/or the Ti interstitials in the passive films can be the main cause for the high values of the donor density. The proposed PDM for Ti and NS Ti-coated samples in H_2SO_4 solutions (as shown in Figure 12) may be best understood when the EIS and M–S analysis results are also considered all at once. As shown in Figure 9, NS Ti-coated samples had thicker passive films compared to Ti in both acid solutions. On the other hand, M–S analysis (Figure 11) indicated that the estimated donor densities of NS Ti-coated sample are lower due to nanostructuring.

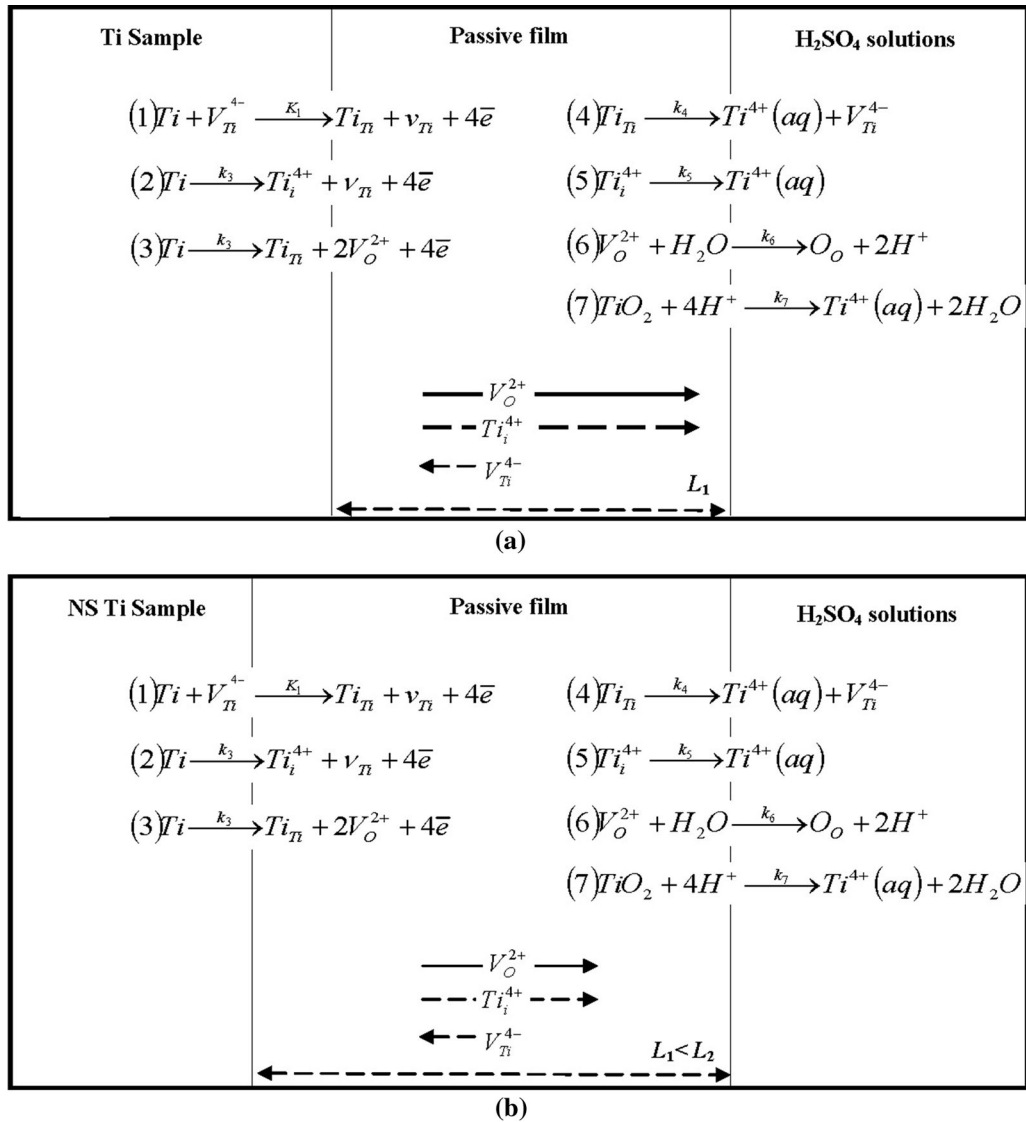


Fig. 12—PDM for the passivation of (a) Ti and (b) nanostructured Ti-coated 304 SS samples in H₂SO₄ solutions; V_{Ti}^{4-} : Ti vacancy on Ti sublattice of passive film; Ti_i^{4+} : interstitial Ti; Ti_{Ti} : Ti cation on Ti sublattice of passive film; V_O^{2+} : oxygen vacancy on the oxygen sublattice of passive film; O_O : oxygen anion on the oxygen sublattice of passive film; $Ti^{4+}(aq)$: Ti cation in solution.

IV. CONCLUSION

CAE was successfully applied to fabricate a NS Ti-coated AISI 304 SS. The effect of nanostructuring of Ti coating on the electrochemical and passive behaviors of the coated sample was investigated thoroughly using a variety of electrochemical techniques in 0.01 and 0.1 M H₂SO₄ solutions. The absence of jumps or abrupt changes in the anodic branch of polarization curves implied that the coating is almost free of common severe defects and protective. In addition, EIS results indicated that NS coating exhibits superior passive behavior. M-S analysis indicated that the passive films behave as n-type semiconductors and nanostructuring did not alter the semiconducting type. Furthermore, our analysis showed that the donor densities are in the order of 10^{21} cm^{-3} and lower for NS coating. Indeed, the obtained results confirmed the formation of a thicker,

yet less defective protective passive film on the surface of NS Ti coating.

REFERENCES

1. J.H. Hsieh, C. Liang, C.H. Yu, and W. Wu: *Surf. Coat. Technol.*, 1998, vols. 108–109, pp. 132–37.
2. F.J. Jing, T.L. Yin, K. Yukimura, H. Sun, Y.X. Leng, and N. Huang: *Vacuum*, 2012, vol. 86, pp. 2114–19.
3. J. Tang, J.S. Zabinski, and J.E. Bultman: *Surf. Coat. Technol.*, 1997, vol. 91, pp. 69–73.
4. S.-Y. Yoon, K.O. Lee, S.S. Kang, and K.H. Kim: *J. Mater. Process. Technol.*, 2002, vols. 130–131, pp. 260–65.
5. B.A. Eizner, G.V. Markov, and A.A. Minevich: *Surf. Coat. Technol.*, 1996, vol. 79, pp. 178–91.
6. B. Podgornik, B. Zajec, N. Bay, and J. Vižintin: *Wear*, 2011, vol. 270, pp. 850–56.

7. C. Liu, Q. Bi, A. Leyland, and A. Matthews: *Corros. Sci.*, 2003, vol. 45, pp. 1257–73.
8. H.A. Jehn: *Surf. Coat. Technol.*, 2000, vol. 125, pp. 212–17.
9. A. Cavaleiro and J.Th.M. De Hosson: in *Nanostructured Coatings*, A. Leyland and A. Matthews, eds., Springer, New York, 2000, pp. 511–38.
10. J.A. Thornton: in *31st Annual Technical Symposium*, M.R. Jacobson, ed., International Society for Optics and Photonics, 1988, pp. 95–105.
11. C.V. Thompson: *Annu. Rev. Mater. Sci.*, 2000, vol. 30, pp. 159–90.
12. A. Bendavid and P.J. Martin: *J. Aust. Ceram. Soc.*, 2014, vol. 50, pp. 86–101.
13. A. Anders: *Surf. Coat. Technol.*, 2014, vol. 257, pp. 308–25.
14. M. Fenker, M. Balzer, and H. Kappl: *Surf. Coat. Technol.*, 2014, vol. 257, pp. 182–205.
15. J. Creus, H. Mazille, and H. Idrissi: *Surf. Coat. Technol.*, 2000, vol. 130, pp. 224–32.
16. C. Liu, G. Lin, D. Yang, and M. Qi: *Surf. Coat. Technol.*, 2006, vol. 200, pp. 4011–16.
17. B.J. Lin, H.T. Zhu, A.K. Tieu, and G. Triani: *Mater. Sci. Forum*, 2013, vols. 773–774, pp. 616–25.
18. S.G. Harris, E.D. Doyle, Y.-C. Wong, P.R. Munroe, J.M. Cairney, and J.M. Long: *Surf. Coat. Technol.*, 2004, vol. 183, pp. 283–94.
19. H. Savaloni, M. Gholipour-Shahraki, and M.A. Player: *J. Phys. D*, 2006, vol. 39, pp. 2231–47.
20. V. Chawla, R. Jayaganthan, A.K. Chawla, and R. Chandra: *J. Mater. Process. Technol.*, 2009, vol. 209, pp. 3444–51.
21. G.T. Burstein: *Corros. Sci.*, 2005, vol. 47, pp. 2858–2870.
22. D.G. Li, J.D. Wang, D.R. Chen, and P. Liang: *Ultrason. Sonochem.*, 2016, vol. 29, pp. 48–54.
23. J. Macdonald, W. Johnson, and J. Macdonald: *Theory in Impedance Spectroscopy*, Wiley, New York, 1987.
24. M. Schönleber, D. Klotz, and E. Ivers-Tiffée: *Electrochim. Acta*, 2014, vol. 131, pp. 20–27.
25. B.A. Boukamp: *Solid State Ion.*, 1993, vol. 62, pp. 131–41.
26. Y. Khelifaoui, M. Kerkar, A. Bali, and F. Dalard: *Surf. Coat. Technol.*, 2006, vol. 200, pp. 4523–29.
27. L. Hamadou, L. Ainouche, A. Kadri, S.A.A. Yahia, and N. Benbrahim: *Electrochim. Acta*, 2013, vol. 113, pp. 99–108.
28. D. Sazou, K. Saltidou, and M. Pagitsas: *Electrochim. Acta*, 2012, vol. 76, pp. 48–61.
29. W. Wang, F. Mohammadi, and A. Alfantazi: *Corros. Sci.*, 2012, vol. 57, pp. 11–21.
30. Z. Jiang, X. Dai, and H. Middleton: *Mater. Chem. Phys.*, 2011, vol. 126, pp. 859–65.
31. B. Roh and D.D. Macdonald: *Russ. J. Electrochem.*, 2007, vol. 43, pp. 125–35.
32. D.D. Macdonald: *Electrochim. Acta*, 2011, vol. 56, pp. 1761–72.
33. D.D. Macdonald: *J. Electrochem. Soc.*, 2006, vol. 153, pp. B213–24.